4232 *Chem. Mater.* **2010,** *22,* 4232–4236
DOI:10.1021/cm100831q

CHEMISTRY OF MATERIALS
Article

# $Mn_3O_4$ Nanocrystals: Facile Synthesis, Controlled Assembly, and Application

Peng Li, Caiyun Nan, Zhe Wei, Jun Lu, Qing Peng, and Yadong Li*

*Department of Chemistry and State Key Laboratory of New Ceramics and Fine Processing, Tsinghua University, Beijing, 100084, People's Republic of China*

*Received March 23, 2010. Revised Manuscript Received June 10, 2010*

We report a facile process for the controllable synthesis of the $Mn_3O_4$ nanocrystals with different sizes and shapes, which includes dots, rods, and wires in the presence of the surfactants dodecanol and oleylamine. It is notable that the uniform-sized nanocrystals were achieved under mild experimental conditions and the common inorganic salt, such as manganese(II) nitrate, was adopted as the precursor. Furthermore, the as-prepared monodisperse nanocrystals, as ideal building blocks, can be rationally assembled into three-dimensional (3D) $Mn_3O_4$ colloidal spheres, using a facile ultrasonication strategy. In particular, the 3D colloidal spheres can be successfully converted to $LiMn_2O_4$ nanocrystals, which show distinct electrochemical performance, mainly depending on their crystallinity and size.

## Introduction

In the past few decades, nanomaterials with controlled size and shape have been investigated in great detail, because of their remarkable physical and chemical properties.[1,2] In particular, because of their unique material properties and potential for desired nanostructures, transition-metal oxide nanocrystals and their assemblies have been widely utilized in various fundamental research and technological applications, such as lithium ion batteries, gas sensors, catalysis, and energy storage.[3−5] Therefore, it is not surprising that long-term endeavors have focused on the synthesis of monodisperse metal oxides nanocrystals and their use as nanobuilding blocks in conveniently constructing ordered superlattice assemblies with advanced functions. Until now, versatile synthetic strategies have been developed to achieve such nanomaterials with tunable sizes and dimensions, including thermolysis of various metallic precursors, the hot-injection method, sol−gel processes, and the reverse-micelle method.[4,6]

Manganese oxides have been the key topics among the transition-metal oxides, because of their potential applications in diverse areas, including rechargeable lithium ion batteries, catalysis, molecular adsorption, and magnetics.[7,8] Until now, a range of methods have been developed to synthesize high-quality monodisperse manganese oxide nanocrystals.[6e,9−11] However, in many cases, the synthetic processes are based on the decomposition of toxic organometallic precursors at high temperatures in

*Author to whom correspondence should be addressed. E-mail: ydli@mail.tsinghua.edu.cn.

(1) (a) Alivisatos, A. P. *Science* **1996**, *271*, 933. (b) Yin, Y. D.; Alivisatos, A. P. *Nature* **2005**, *437*, 664. (c) Murray, C. B.; Kagan, C. R.; Bawendi, M. G. *Annu. Rev. Mater. Sci.* **2000**, *30*, 545. (d) Cui, Y.; Lieber, C. M. *Science* **2001**, *291*, 851.
(2) (a) Peng, X. G.; Manna, L.; Yang, W. D.; Wickham, J.; Scher, E.; Kadavanich, A.; Alivisatos, A. P. *Nature* **2000**, *404*, 59. (b) Zeng, H.; Li, J.; Liu, J. P.; Wang, Z. L.; Sun, S. H. *Nature* **2002**, *420*, 395. (c) Chan, W. C. W.; Nie, S. M. *Science* **1998**, *281*, 2016. (d) Wang, X.; Zhuang, J.; Peng, Q.; Li, Y. D. *Nature* **2005**, *437*, 121.
(3) (a) Nardi, J. C. *J. Electrochem. Soc.* **1985**, *132*, 1787. (b) Armstrong, A. R.; Bruce, P. G. *Nature* **1996**, *381*, 499. (c) Nayral, C.; Viala, E.; Fau, P.; Senocq, F.; Jumas, J.-C.; Maisonnat, A.; Chaudret, B. *Chem.—Eur. J.* **2000**, *6*, 4082. (d) Zarur, A. J.; Ying, J. Y. *Nature* **2000**, *403*, 65. (e) Hu, L. H.; Peng, Q.; Li, Y. D. *J. Am. Chem. Soc.* **2008**, *130*, 16136.
(4) Sun, S. H.; Zeng, H. *J. Am. Chem. Soc.* **2002**, *124*, 8204.
(5) (a) Ge, J. P.; Hu, Y. X.; Biasini, M.; Beyermann, W. P.; Yin, Y. D. *Angew. Chem.* **2007**, *119*, 4420. (b) Angew. Chem., Int. Ed. **2007**, *46*, 4342.
(6) (a) Sun, S. H.; Zeng, H.; Robinson, D. B.; Raoux, S.; Rice, P. M.; Wang, S. X.; Li, G. *J. Am. Chem. Soc.* **2004**, *126*, 273. (b) Park, J.; An, K.; Hwang, Y.; Park, J.-G.; Noh, H.-J.; Kim, J.-Y.; Park, J.-H.; Hwang, N.-M.; Hyeon, T. *Nat. Mater.* **2004**, *3*, 891. (c) Wang, D. S.; Xie, T.; Peng, Q.; Zhang, S. Y.; Chen, J.; Li, Y. D. *Chem.—Eur. J.* **2008**, *14*, 2507. (d) Rockenberger, J.; Scher, E. C.; Alivisatos, A. P. *J. Am. Chem. Soc.* **1999**, *121*, 11595. (e) Wang, N.; Guo, L.; He, L.; Cao, X.; Chen, C. P.; Wang, R. M.; Yang, S. H. *Small* **2007**, *4*, 606. (f) Ngo, A.-T.; Pileni, M. P. *Adv. Mater.* **2000**, *12*, 276.
(7) Kim, D. K.; Muralidharan, P.; Lee, H. -W.; Ruffo, R.; Yang, Y.; Chan, C. K.; Peng, H.; Huggins, R. A.; Cui, Y. *Nano Lett.* **2008**, *8*, 3948.
(8) (a) Hosono, E.; Kudo, T.; Honma, I.; Matsuda, H.; Zhou, H. *Nano Lett.* **2009**, *9*, 1045. (b) Grootendorst, E.; Verbeek, Y.; Ponce, V. *J. Catal.* **1995**, *157*, 706. (c) Shen, Y. F.; Zerger, R. P.; Deguzman, R. N.; Suib, S. L.; Mccurdy, L.; Potter, D. I.; O'Young, C. L. *Science* **1993**, *260*, 511. (d) Park, J.; Kang, E.; Bae, C. J.; Park, J. G.; Noh, H. J.; Kim, J. Y.; Park, J. H.; Park, H. M.; Hyeon, T. *J. Phys. Chem. B* **2004**, *108*, 13594. (e) Jiao, F.; Harrison, A.; Hill, A. H.; Bruce, P. G. *Adv. Mater.* **2007**, *19*, 4063. (f) Seo, W. S.; Jo, H. H.; Lee, K.; Kim, B.; Oh, S. J.; Park, J. T. *Angew. Chem., Int. Ed.* **2004**, *43*, 1115. (g) Lei, S. J.; Tang, K. B.; Fang, Z.; Zheng, H. G. *Cryst. Growth Des.* **2006**, *6*, 1757.
(9) Jana, N. R.; Chen, Y. F.; Peng, X. G. *Chem. Mater.* **2004**, *16*, 3931.
(10) (a) Narayanaswamy, A.; Xu, H. F.; Pradhan, N.; Kim, M.; Peng, X. G. *J. Am. Chem. Soc.* **2006**, *128*, 10310. (b) Wang, W. Z; Xu, C. K.; Wang, G. H.; Liu, Y. K.; Zheng, C. L. *Adv. Mater.* **2002**, *14*, 837. (c) Yin, M.; O'Brien, S. *J. Am. Chem. Soc.* **2003**, *125*, 10180. (d) Yu, T.; Moon, J.; Park, J.; Park, Y. I.; Na, H. B.; Kim, B. H.; Song, I. C.; Moon, W. K.; Hyeon, T. *Chem. Mater.* **2009**, *21*, 2272. (e) Zhao, N. N.; Nie, W.; Liu, X. B.; Tian, S. Z.; Zhang, Y.; Ji, X. L. *Small* **2008**, *4*, 77. (f) Du, Y. P.; Zhang, Y. W.; Sun, L. D.; Yan, C. H. *J. Phys. Chem. C* **2009**, *113*, 6521. (g) Salazar-Alvarez, G.; Sort, J.; Suriach, S.; Bar, M. D.; Nogues, J. *J. Am. Chem. Soc.* **2007**, *129*, 9102.
(11) Chen, Y. F.; Johnson, E.; Peng, X. G. *J. Am. Chem. Soc.* **2007**, *129*, 10937.


Published on Web 07/02/2010

hazardous coordinating solvent systems. Furthermore, only a few methods have been devised to synthesize $Mn_3O_4$ nanomaterials with one or more dimensions. Recently, our group developed a selected-control low-temperature hydrothermal method to synthesize one-dimensional (1D) $MnO_2$ nanostructures.[12] In this paper, we present a facile one-step synthetic route to achieve uniformly sized $Mn_3O_4$ nanocrystals with high yield and distinct shapes of dots, rods, and wires. It is noteworthy that the as-prepared nanocrystals were obtained under mild experimental conditions and the common inorganic salt, such as manganese(II) nitrate, was adopted as the precursor. Moreover, the as-prepared hydrophobic spherical or elongated nanoparticles were used as building blocks to be rationally assembled into three-dimensional (3D) $Mn_3O_4$ colloidal spheres with a facile ultrasonication strategy. In addition, for further electrochemical application, the colloidal spheres were chemically converted to $LiMn_2O_4$ nanomaterials in a simple solid-state reaction. More importantly, the as-obtained nanocrystals showed distinct electrochemical performance.

## Experimental Section

**Synthesis.** $Mn_3O_4$ nanocrystals were prepared via a hydrothermal method in 10-mL Teflon-lined autoclaves. A typical synthesis of $Mn_3O_4$ nanocrystals was as follows:

For almost-spherical $Mn_3O_4$ nanoparticles: 1 mL $Mn(NO_3)_2$ solution (50 wt %) was added to the 10-mL autoclave containing 9 mL oleylamine under agitation. Then, the above solution was sealed, and hydrothermally treated at 200 °C for 24 h. After the reaction was cooled to room temperature, the products were washed with ethanol and then dispersed in nonpolar solvents. For the elongated nanoparticles, 1 mL $Mn(NO_3)_2$ (50 wt %) (or 500 $\mu$L) was added to the mixed solution containing 5 mL dodecanol and 4 mL oleylamine (or 2 mL dodecanol + 3 mL oleylamine) under agitation, followed by heating at 200 °C for 10 h, respectively.

For $Mn_3O_4$ nanorods: Typically, 1 mL of $Mn(NO_3)_2$ solution (50 wt %) was dissolved in the mixed solution containing 3 mL of dodecanol and 6 mL of oleylamine under stirring and hydrothermally treated at 200 °C for 10 h. Short rods were also obtained when 2 mL of $Mn(NO_3)_2$ solution was added into 8 mL of oleylamine at ~200 °C for 5−10 h.

For $Mn_3O_4$ nanowires: Briefly, 400 or 250 $\mu$L of $Mn(NO_3)_2$ solution (50 wt %) was added to the mixed solution containing 6 mL of dodecanol and 3 mL of oleylamine under stirring and hydrothermally treated at ~170 °C for 10 h.

*Synthesis of $Mn_3O_4$ Colloidal Spheres.* Ten milliliters of the as-prepared $Mn_3O_4$ nanocrystals solution (~10 mg/mL in hexane) was injected into 100 mL of sodium dodecylsulfonate (SDS) solution (1 mol/L). The mixed solution then was magnetically stirred at 5000 rpm for 1 h. The colloidal spheres were obtained after the above solution was heated at 70 °C for 2−3 h to evaporate the hexane. The final products were obtained by centrifuging.

*Synthesis of $LiMn_2O_4$ Nanocrystals.* Typically, $LiOH \cdot H_2O$ and the as-prepared $Mn_3O_4$ colloidal spheres, mixed with a molar ratio, were added into 3 mL of high-purity ethanol under agitation and dried at room temperature. The mixed powder was then calcined at 450−750 °C in air for several hours.

(12) Wang, X.; Li, Y. D. *J. Am. Chem. Soc.* **2002**, *124*, 2880.

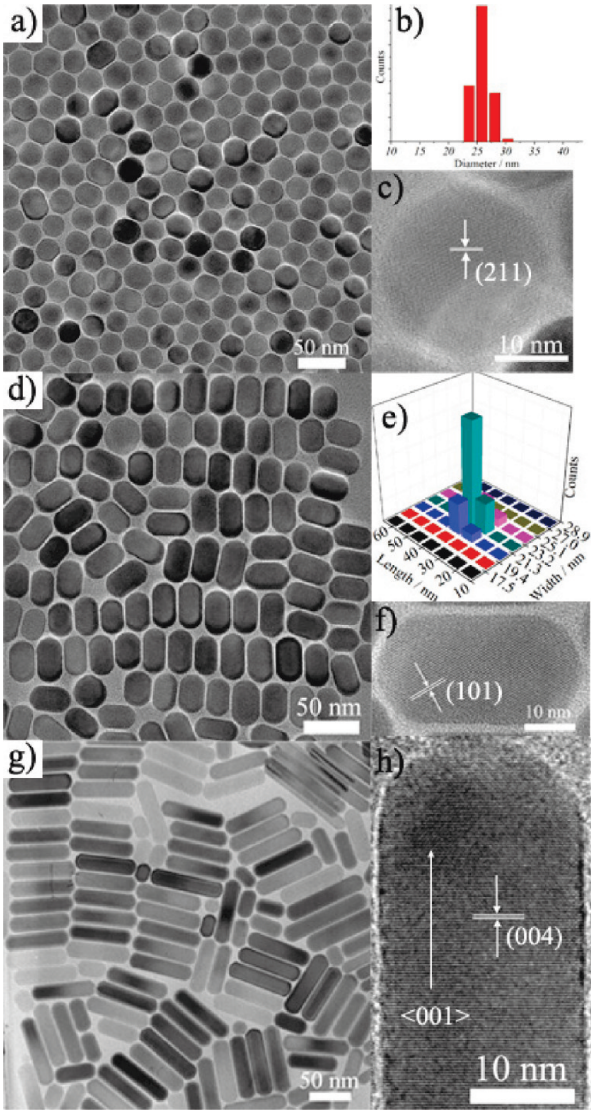


**Figure 1.** TEM images of the as-prepared samples: (a) TEM image, (b) size distribution, and (c) HRTEM image of the spherical $Mn_3O_4$ nanoparticles; (d) TEM image, (e) size distribution, and (f) HRTEM image of the elongated $Mn_3O_4$ nanocrystals; and (g) TEM image and (h) HRTEM image of the short $Mn_3O_4$ nanorods.

**Electrochemical Investigation.** Electrochemical measurements were performed using coin-type cells. The working electrode was constructed by making a slurry of the active material, acetylene black, and polyvinylidene fluoride (PTFE), using a weight ratio of 80:10:10. Lithium metal was used as the counter electrodes, and the separator was a Celgard 2300 microporous membrane. A 1 mol/L solution of $LiPF_6$ dissolved in the mixture of ethylene carbonate/dimethyl carbonate (EC/DMC), with a 1:1 volume ratio, was used as the electrolyte. Cell assembly was carried out in a glovebox filled with high-purity argon gas. The charge/discharge tests were performed within a range of 3.0−4.3 V at different current densities.

**Characterization.** The phase purity of the products were examined on a Bruker Model D8 Advance X-ray powder diffractometer with Cu K$\alpha$ radiation ($\lambda$ = 1.5418 Å). The size and morphology of the products were determined by transmission electron microscopy (TEM) (JEOL Model JEM 1200EX, operating at an accelerating voltage of 100 kV), scanning electron microscopy (SEM) and high-resolution TEM (HRTEM) (FEI Tecnai Model G2 F20 S-Twin, operating at an accelerating voltage of 200 kV).

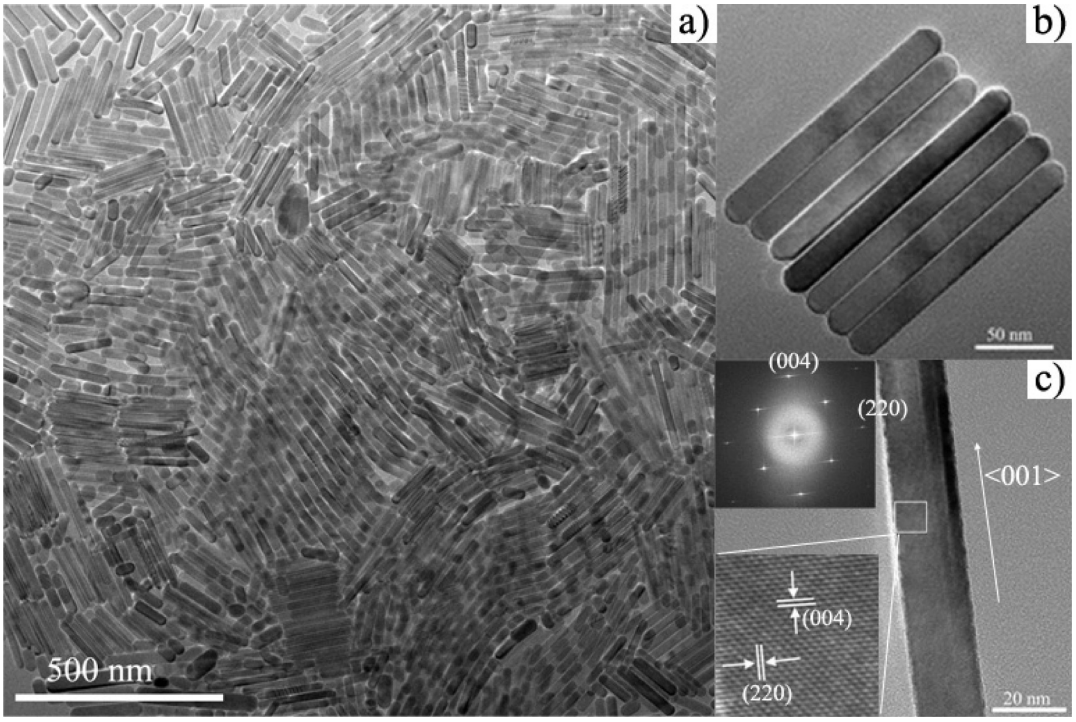


**Figure 2.** Typical TEM images of the long $Mn_3O_4$ nanorods: (a, b) low-resolution TEM images of the obtained nanorods; (c) high-resolution TEM image of an individual rod (the inset at the bottom is a magnified image of the lattice fringe and the inset at the top is the corresponding FFT pattern of the rod. According to the HRTEM image and the FFT, the nanorod's growth direction is ⟨001⟩.

## Results and Discussion

In our synthetic process, $Mn_3O_4$ nanocrystals with various sizes and shapes are achieved under different conditions (see Experimental Section for details). Figure 1 shows the typical TEM image of the as-obtained $Mn_3O_4$ nanoparticles. Almost-spherical $Mn_3O_4$ nanoparticles are obtained in the presence of oleylamine. Figure1a shows that the average diameter is 25.9 ± 1.4 nm. Notably, the almost-monodisperse nanoparticles possess a narrow size distribution (Figure 1b). The HRTEM image shown in Figure 1c clearly reveals the highly crystalline nature. The lattice fringe spacing corresponds to the (211) plane of tetragonal $Mn_3O_4$ nanoparticles. In contrast, with increasing $Mn^{2+}$ concentration (2 mL) and shortening the reaction time, $Mn_3O_4$ nanocrystals with rodlike morphology are also obtained. Figure 1g indicates that most of the $Mn_3O_4$ nanorods are ~20 nm in diameter and ~80 nm in length, with an aspect ratio of ~4. The HRTEM image (Figure 1h) illustrates that the alkylamines selectively bind to the surfaces of crystallites and render the epitaxial growth along the ⟨001⟩ directions.

To investigate the dependency of surfactants on the morphology of the nanocrystals, the mixed solvents of dodecanol and oleylamine are also employed. In this case, upon varying the volume and composition of the solvent, the size and shape of $Mn_3O_4$ nanocrystals can be tuned. As shown in Figures 1d−f, elongated $Mn_3O_4$ nanoparticles are obtained with a width of 22.2 ± 0.9 nm and a length of 36.7 ± 3.6 nm. The HRTEM image (Figure 1f) indicates that the elongated nanocrystals have good crystallinity. In contrast, long $Mn_3O_4$ nanorods with the aspect ratio of ~9 are achieved in the presence of 3 mL of dodecanol and 6 mL of oleylamine. Figure 2 shows the TEM images of the obtained nanocrystals. The length of the $Mn_3O_4$ nanorods increases to ~180 nm and the diameter is ~20 nm. The HRTEM image of the individual nanorod (Figure 2c) shows that the growth direction is along the ⟨001⟩ direction. The fast Fourier transform (FFT) pattern (the inset) is also consistent with the results. Moreover, a decrease in the reaction temperature (down to ~170 °C) can result in the formation of ultralong nanowires (more than 20 $\mu$m) with uniform diameters of ~12 nm (Figure 3). Figure S4 in the Supporting Information shows the energy-dispersive X-ray spectrum (EDS) of the obtained nanowires. Meanwhile, uniform $Mn_3O_4$ nanorods with a width of ~10 nm and a length of ~30 nm are also obtained (see Figure S5 in the Supporting Information). Figure S1 in the Supporting Information shows the powder XRD patterns of the as-obtained nanocrystals. All the peaks are in agreement with the tetragonal phase of $Mn_3O_4$ (JCPDS File Card No. 24-0734).

Based on the experimental results, we may propose the nucleation and growth mechanism of $Mn_3O_4$ nanocrystals. In our system, oleylamine seems to play a crucial factor as an alkalescent medium. When $Mn^{2+}$ was added to the sole solvent of oleylamine at a relatively lower temperature for several hours, $Mn(OH)_2$ nanoparticles could be obtained (see Figure S2 in the Supporting Information). Therefore, we assume that, with the injection of the aqueous solution of $Mn^{2+}$, the nuclei of $Mn(OH)_2$ were formed in the presence of oleylamine at the early stage, followed by the nucleation of $Mn_3O_4$ nanocrystals, because of the presence of $H_2O$ under the

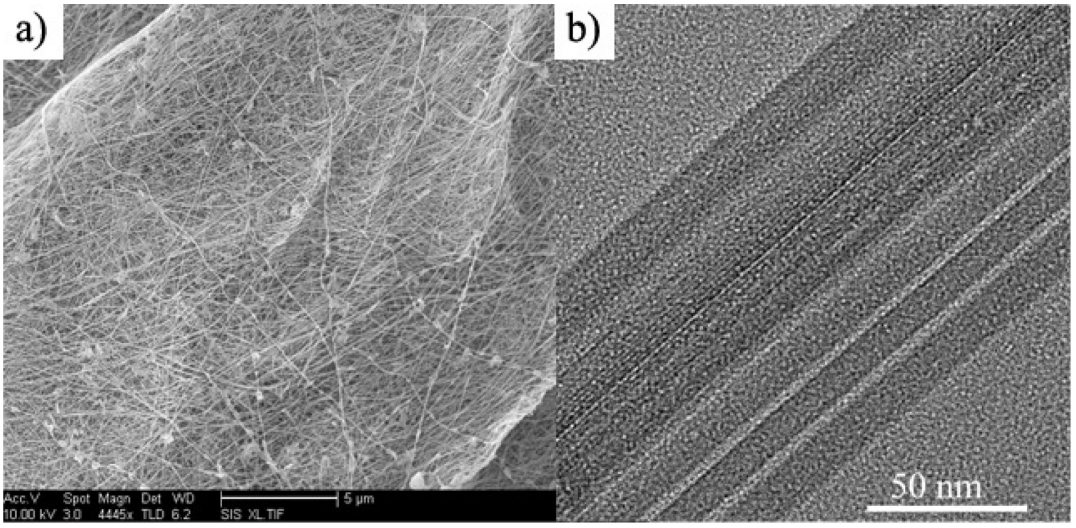


**Figure 3.** (a) SEM image and (b) TEM image of the as-obtained ultralong $Mn_3O_4$ nanowires.

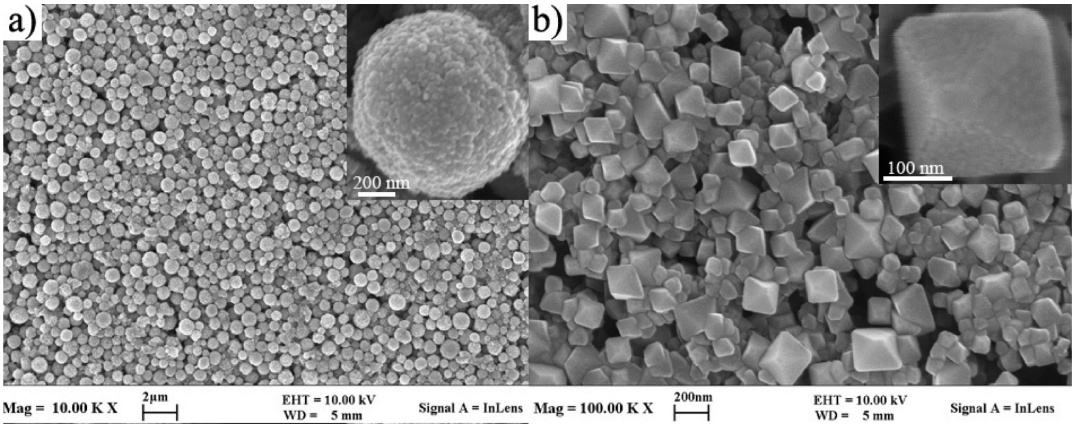


**Figure 4.** SEM images of (a) the as-prepared 3D $Mn_3O_4$ colloidal spheres and (b) $LiMn_2O_4$ with octahedron-like morphology.

elevated temperatures. In our experiment, maintaining a sufficient concentration of $Mn^{2+}$ is favorable to the preferential growth of $Mn_3O_4$ nanorods along the ⟨001⟩ directions. To our knowledge, surface energy plays a vital role in the anisotropic growth of the nanomaterials and the growth rate is exponentially proportional to the surface energy under the kinetic growth process.[13] The experimental results revealed that the selective adsorption of surfactants onto the lower energy surfaces leads to the formation of the $Mn_3O_4$ nanorods or elongated nanoparticles, which has a {001} surface with higher energy.[13] However, we found that, with increased annealing time, most of the as-prepared $Mn_3O_4$ nanorods eventually were converted to dotlike nanoparticles. The experimental results indicated that dotlike shapes are thermodynamically more stable, compared to the rodlike shapes, which is in accord with the results by Peng's group.[11,14] Meanwhile, in our experiment, both oleylamine and dodecanol act as the structure-directing agents, which largely affect the monodispersity and morphology of the as-prepared nanocrystals. The solvent composition plays a critical role in the system. Upon appropriately increasing the amount of dodecanol at lower temperature, the nucleation process seems to be limited, and, thus, the growth process will be accelerated, leading to the formation of $Mn_3O_4$ nanowires.

Using the emulsion-based bottom-up self-assembly approach,[15] we can fabricate 3D $Mn_3O_4$ colloidal spheres, using the as-prepared monodisperse spherical or elongated nanoparticles as building blocks. Figure 4a shows the typical SEM image of $Mn_3O_4$ colloidal spheres with an average diameter of ~1 $\mu$m. Moreover, we further investigated their electrochemical application in lithium ion batteries. To our knowledge, the $LiMn_2O_4$ is one of the most promising candidates as a cathode material, because of its low cost, environmental friendliness, and high abundance, in comparison to commercial $LiCoO_2$.[7,8a] Notably, the as-prepared $Mn_3O_4$ colloidal spheres can be successfully converted to $LiMn_2O_4$ nanocrystals via a simple solid-state reaction (see Experimental Section for details). Interestingly, novel-shaped $LiMn_2O_4$ can be tuned during the process.

(13) Seo, J.-W.; Jun, Y.-W.; Ko, S. J.; Cheon, J. *J. Phys. Chem. B* **2005**, *109*, 5389.
(14) (a) Peng, Z. A.; Peng, X. G. *J. Am. Chem. Soc.* **2001**, *123*, 1389. (b) Peng, Z. A.; Peng, X. G. *J. Am. Chem. Soc.* **2002**, *124*, 3343.
(15) (a) Bai, F.; Wang, D. S.; Huo, Z. Y.; Chen, W.; Liu, L. P.; Liang, X.; Chen, C.; Wang, X.; Peng, Q.; Li, Y. D. *Angew. Chem.* **2007**, *119*, 6770. (b) Angew. Chem., Int. Ed. **2007**, *46*, 6650.

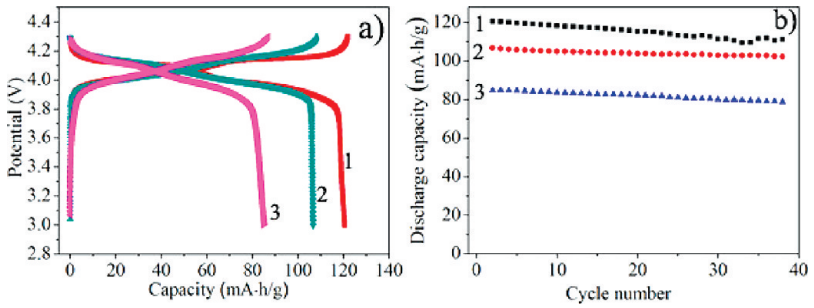


**Figure 5.** (a) Charge−discharge curves at the second cycle at a rate of 0.1 C. (b) Discharge capacity curve versus the number of cycles for $LiMn_2O_4$ nanocrystals at a rate of 0.1 C. (The labels "1", "2", and "3" in the figure represent the results from the octahedron-like, commercial, and spherical $LiMn_2O_4$ samples, respectively.)

When the mixed powder of $Mn_3O_4$ colloidal spheres and $LiOH \cdot H_2O$ is sintered at a temperature of ~450 °C for 2 h, the morphology of the obtained $LiMn_2O_4$ mainly remained spherical (shown in Figure S6a in the Supporting Information). However, upon increasing the reaction temperature to ~700 °C, the SEM image (Figure 4b) shows that $LiMn_2O_4$ with an octahedron-like morphology can be produced. Meanwhile, the aggregation of small octahedron-like particles is also observed (the area highlighted by the arrow in Figure S6b in the Supporting Information).

The XRD patterns are in good agreement with the standard pattern for $LiMn_2O_4$ (JCPDS File Card No. 35-0782), with no peaks of the $Mn_3O_4$ phase detected (see Figure S3 in the Supporting Information). Figure 5a shows the charge−discharge curves at a constant rate (0.1 C). The octahedron-like $LiMn_2O_4$ sintered at ~700 °C shows higher capacity, compared to that of the commercial samples. However, the $LiMn_2O_4$ with spherical structures, which was sintered at ~450 °C, shows the large potential drops and a nonflat plateau. Furthermore, the discharge capacities and cycle stability of the materials were also compared under the same conditions. Figure 5b shows that the octahedron-like particles exhibit a much higher charge capacity than the spherical structure. To our knowledge, the morphology seems to be crucial to understanding the electrochemical performance.[7,8a,16] In our experiment, $LiMn_2O_4$ nanocrystals were obtained at different sintering temperatures. Hence, the different electrochemical properties may mainly pertain to the crystallinity quality and size of the nanomaterials.

(16) (a) Wang, D. S.; Ma, X. L.; Wang, Y. G.; Wang, L.; Wang, Z. Y.; Zheng, W.; He, X. M.; Li, J.; Peng, Q.; Li, Y. D. *Nano Res.* **2010**, *3*, 1. (b) Xiao, X. L.; Wang, L.; Wang, D. S.; He, X. M.; Peng, Q.; Li, Y. D. *Nano Res.* **2009**, *2*, 923.

## Conclusion

In conclusion, a facile method has been successfully developed for the synthesis of $Mn_3O_4$ nanocrystals with the shapes of dots, rods, and wires. Moreover, the resulting highly monodisperse nanocrystals can be assembled into three-dimensional (3D) colloidal spheres. For further electrochemical application, the as-prepared colloidal spheres were chemically converted to $LiMn_2O_4$ nanomaterials in a simple solid-state reaction. More interestingly, the as-obtained nanocrystals showed different electrochemical performance mainly depending on the crystallinity and size. We hope that these results will help to understand and precisely control the shape of many other metal oxide nanocrystals for constructing functional macroscopic architectures or devices.

**Acknowledgment.** This work was supported by the NSFC (Nos. 20921001, 90606006), the State Key Project of Fundamental Research for Nanoscience and Nanotechnology (No. 2006CB932300).

**Supporting Information Available:** XRD patterns, EDS, and additional TEM images. (PDF) This material is available free of charge via the Internet at http://pubs.acs.org.